Bioactive Materials 6 (2021) 3568–3579

Contents lists available at ScienceDirect

Bioactive Materials

journal homepage: www.sciencedirect.com/journal/bioactive-materials

Injectable kartogenin and apocynin loaded micelle enhances the alleviation of intervertebral disc degeneration by adipose-derived stem cell

Chao Yu [a,b,c,1], Dongdong Li [d,1], Chenggui Wang [a,b,c,1], Kaishun Xia [a,b,c], Jingkai Wang [a,b,c], Xiaopeng Zhou [a,b,c], Liwei Ying [a,b,c], Jiawei Shu [a,b,c], Xianpeng Huang [a,b,c], Haibin Xu [a,b,c], Bin Han [a,b,c], Qixin Chen [a,b,c], Fangcai Li [a,b,c,***], Jianbin Tang [d,**], Chengzhen Liang [a,b,c,*], Nigel Slater [e]

[a] Department of Orthopedics Surgery, The Second Affiliated Hospital, Zhejiang University School of Medicine, Hangzhou City, Zhejiang Province, PR China
[b] Orthopedics Research Institute of Zhejiang University, Hangzhou City, Zhejiang Province, PR China
[c] Key Laboratory of Motor System Disease Research and Precision Therapy of Zhejiang Province, Hangzhou City, Zhejiang Province, PR China
[d] Key Laboratory of Biomass Chemical Engineering of Ministry of Education, Center for Bionanoengineering, and College of Chemical and Biological Engineering, Zhejiang University, Hangzhou, Zhejiang, 310027, China
[e] Department of Chemical Engineering and Biotechnology, University of Cambridge, Cambridge, United Kingdom

ARTICLE INFO

Keywords:
Intervertebral disc degeneration
Polymer-drug conjugates
Mesenchymal stem cell
Reactive oxygen species
Stem cell therapy

ABSTRACT

Cell transplantation has been proved the promising therapeutic effects on intervertebral disc degeneration (IVDD). However, the increased levels of reactive oxygen species (ROS) in the degenerated region will impede the efficiency of human adipose-derived stem cells (human ADSCs) transplantation therapy. It inhibits human ADSCs proliferation, and increases human ADSCs apoptosis. Herein, we firstly devised a novel amphiphilic copolymer PEG-PAPO, which could self-assemble into a nanosized micelle and load lipophilic kartogenin (KGN), as a single complex (PAKM). It was an injectable esterase-responsive micelle, and showed controlled release ability of KGN and apocynin (APO). Oxidative stimulation promoted the esterase activity in human ADSCs, which accelerate degradation of esterase-responsive micelle. Compared its monomer, the PAKM micelle possessed better bioactivities, which were attributed to their synergistic effect. It enhanced the viability, autophagic activation (P62, LC3 II), ECM-related transcription factor (SOX9), and ECM (Collagen II, Aggrecan) maintenance in human ADSCs. Furthermore, it is demonstrated that the injection of PAKM with human ADSCs yielded higher disc height and water content in rats. Therefore, PAKM micelles perform promoting cell survival and differentiation effects, and may be a potential therapeutic agent for IVDD.

1. Introduction

Intervertebral disc degeneration (IVDD) is the main cause of lower back pain, which can create high medical expenses [1,2]. The nucleus pulposus (NP), annulus fibrosus, and endplate are the important components in intervertebral disc (IVD) [3]. Annulus fibrosus is made up of a series of 15–25 concentric rings, or lamellae, with the collagen fibers lying parallel within each lamella. Endplate is a thin horizontal layer of hyaline cartilage, which interfaces the disc and the vertebral body. The NP is a fiber reinforced, isotropic, gelatinous, water-rich, and swollen core, which is the main structure in IVD. It provides compressive resistance as well as a center of rotation for movement [4,5]. Many

Peer review under responsibility of KeAi Communications Co., Ltd.

* Corresponding author. Department of Orthopedics Surgery, The Second Affiliated Hospital, Zhejiang University School of Medicine, Hangzhou City, Zhejiang Province, PR China.

** Corresponding author. Key Laboratory of Biomass Chemical Engineering of Ministry of Education, Center for Bionanoengineering, and College of Chemical and Biological Engineering, Zhejiang University, Hangzhou, Zhejiang, 310027, China.

*** Corresponding author. Department of Orthopedics Surgery, The Second Affiliated Hospital, Zhejiang University School of Medicine, Hangzhou City, Zhejiang Province, PR China.

E-mail addresses: lifangcai@zju.edu.cn (F. Li), jianbin@zju.edu.cn (J. Tang), liangchengzhen@zju.edu.cn (C. Liang).

[1] Chao Yu, Dongdong Li, and Chenggui Wang contributed equally to this work.

https://doi.org/10.1016/j.bioactmat.2021.03.018
Received 3 November 2020; Received in revised form 20 February 2021; Accepted 6 March 2021

pathological factors, including aging, trauma, genetics or other exogenous stimuli result in IVDD [6]. Meanwhile, IVDD is characterized by various structural and histological changes as well as an altered expression of extracellular matrix (ECM) and inflammatory markers [7].

In the past decade, supplementation of exogenous human adipose mesenchymal stem cells (human ADSCs) has shown therapeutic effects on IVDD in both basic research and preclinical studies [6,8,9]. First, the NP area is recognized as an immune privileged region. This characteristic limits immune responses to exogenous stem cell transplantation [10]. Transplantation of pre-differentiated human ADSCs can also augment the number of functional cells and ECM, thus maintaining IVD functions [11,12]. Therefore, exogenous human ADSCs transplantation is a promising treatment target for IVDD repair [9]. However, the efficiency of cell differentiation and survival rate of transplanted cells in IVD are major obstacles. After stem-cell transplantation, many injected cells rapidly become undetectable, suggesting that the viability and functionality of these cells might be dramatically damaged [6,8,13]. The main reason for this is the harsh microenvironment caused by nonspecific inflammation and excessive reactive oxygen species (ROS) at the lesion site [14]. Excessive ROS levels in the degenerated area inhibits human ADSCs proliferation, increases apoptosis, and reduces the efficiency of IVDD treatment. Oxidative stress also causes hyper-peroxidation, protein carbonylation, and DNA damage to human ADSCs [15,16]. Consequently, it is necessary to find methods to decrease ROS levels in the degenerated disc microenvironment to facilitate the viability and functionality of human ADSCs.

To solve these therapeutic problems, an esterase-responsive apocynin (APO)-based amphiphilic polymer micelle loaded with kartogenin (KGN), as a single complex (PAKM), was designed for IVDD treatment. The PAKM provided sustained delivery of KGN and APO in a single system. APO is a naturally occurring methoxy-substituted catechol, used experimentally as an NADPH oxidase inhibitor [17,18]. Its antioxidant effects arise through its inhibition of translocation of the cytosolic component p47phox of the NADPH-oxidase complex to the cell membrane [19–22]. Several studies have shown that pretreatment with APO facilitates the therapeutic efficacy of stem cells by improving the anti-aging and anti-apoptotic capability [23,24]. Meanwhile, lipophilic KGN were loaded in the micelle. Others have shown that stem cells induced by KGN could differentiate into an NP-like phenotype, and contribute to attenuation of intervertebral disc degeneration [25]. Therefore, we suppose that APO stimulate the proliferation and survival rate of human ADSCs, which could be further developed into an NP-like phenotype by KGN. The combination of APO and KGN might have a synergetic effect in ameliorating the function of the degenerative disc. However, the delivery of APO and KGN into the NP area still faces obstacles due to the lack of vascularization of the intervertebral disc and the short-lived effect of the bioactive agents. Focus has been shifted towards an injectable delivery system with advantages such as prolonged biological drug activity, lower systemic drug concentrations, and decreased administration frequencies. Herein, a polymer micelle-based drug delivery system was developed, in which the APO drug is linked onto the polymer chain via an esterase-responsive phenolic ester bond and KGN was physically loaded in the core of the micelle. Transplanted human ADSCs increased esterase activity under oxidative stress, initiating APO and KGN release at the disc lesion site. Overall, PAKM showed an accurate and controlled delivery of the APO and KGN, which protects human ADSCs from oxidative stress and promotes human ADSCs to differentiate into an NP-like phenotype (see Scheme 1).

2. Materials and methods

2.1. Materials

2-hydroxyethyl methacrylate (HEMA), triphosgene, 2-hydroxyethyl methacrylate (HEMA), apocynin (APO), kartogenin (KGN), 1-(3-Dimethylaminopropyl)-3-ethylcarbodiimide hydrochloride (EDC), 4-dimethylaminopyridine (DMAP), 2-Hydroxy-2-methylpropiophenone and 2, 2′-azobis (2-methylpropionitrile) (AIBN), polyethyleneglycol (PEG5000-OH) were purchased from Energy Chemical (Shanghai, China).

2.2. Synthesis of PEG-PETTC

4-Cyano-4-(2-phenylethanesulfanylthiocarbonyl) sulfanylpentanoic Acid (PETTC, 1.02 g, 0.003 mol) was prepared according to the literature [26], PEG5000-OH (5 g, 0.001 mol), DMAP (0.12 g, 0.001 mol) were dissolved in 100 mL DCM, EDC (0.86 g, 0.0045 mol) was dropwise added into the above solution under ice bath. After 24 h at room temperature, the DCM was removed and the mixture was precipitated in diethyl ether. The obtained product was light yellow solid (3.8g, 71%)

2.3. Synthesis of monomer 2-(((4-acetyl-2-methoxyphenoxy)carbonyl) oxy)ethyl methacrylate (HAPO)

Hydroxyethyl methacrylate (HEMA, 3.9 g, 0.03 mmol), triphosgene (2.97 g, 0.01 mol) was dissolved in 50 mL THF, and triethylamine (3 g, 0.03 mol) in dry THF (10 mL) was added into the above solution at 0 °C. After 1 h, triethylamine hydrochloride was removed by filtering, and the

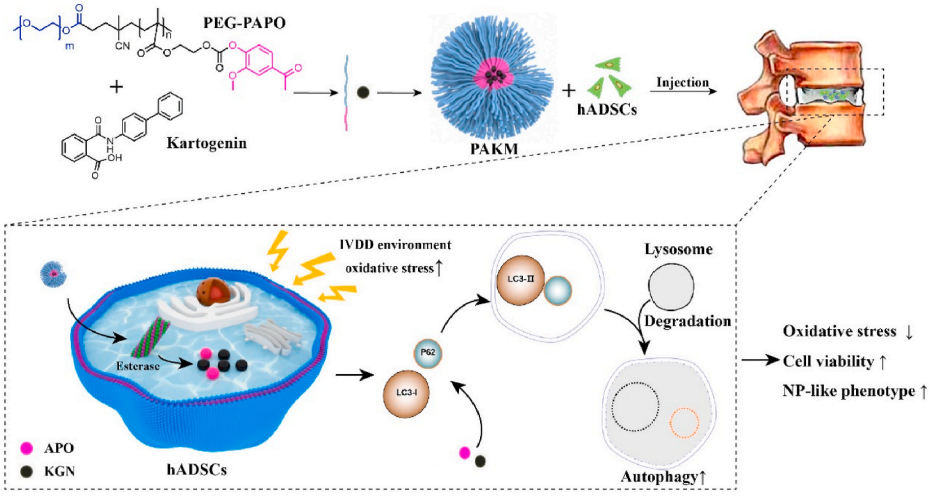

Scheme 1. General schematic of synthesis of an injectable and degradable antioxidant polymer micelle (PAKM) as stem cell therapy for intervertebral disc degeneration. human ADSCs is represented by hADSCs as follow: hADSCs = Human ADSCs.

solution was mixed with apocynin (APO, 5 g, 0.03 mol), and triethylamine (3 g, 0.03 mol) in dry THF (10 mL) was added into the solution at 0 °C, the reaction was conducted at room temperature for 24 h. After removing the triethylamine hydrochloride by filtration, THF was removed by rotary evaporation, and the crude product was washed with 1 M HCl and brine, and purified by column chromatography (silica gel, hexane: ethyl acetate = 3:1) to afford 8.2 g (84.5%). ^{1}H NMR (400 MHz, $CDCl_3$) δ = 7.66–7.49 (m, 2 H), 7.24 (m, 1 H), 6.2 (3, 1 H), 5.6 (s, 0 H), 4.49 (m, 3 H), 3.91 (s, 3 H), 2.61 (s, 3 H), 2.00 (s, 3 H).

2.4. Synthesis of block copolymer PEG-PAPO

PEG-PETTC (0.20 g, 0.037 mmol), HAPO (0.20 g, 0.6 mmol), AIBN (6.56 mg, 0.04 mmol), and DMF (2 mL) were charged into a Schlenk tube with a magnet. After removing the O_2 by N_2, the reaction was heated to 70 °C for 15 h. PEG-PAPO was obtained by precipitating in diethyl ether. (0.23g 57.5%) ^{1}H NMR (400 MHz, DMSO) δ 7.55 (32H), 7.26 (6H), 4.24 (64 H), 3.80 (48 H), 3.51 (454 H), 2.53 (48 H).

2.5. Preparation and characterization of the micelle

DMSO (0.5 mL) was used to dissolved PEG-PAPO (40 mg) and KGN (4 mg). The solution was dropwise added into deionized water (8 mL) with strong stirring, and DMSO was removed by dialyzing. Dynamic light scattering (DLS) spectrometer (Nano series ZEN3600, Malvern Instruments Ltd., UK) was used to characterize the size and morphology of the micelles.

2.6. Esterase degradation measurement

The micelle was dissolved in PBS and divided into pH 7.4 group and pH 7.4 with esterase (120 U/mL) group. A nanoparticle solution for each group (1 mL, containing 10 mg polymer) and esterase were sealed in a dialysis bag with a molecular weight cut off at 3500 Da and dialyzed in 39 mL of PBS with 2% Tween 80. At regular intervals, a 200 μL of liquid outside the bag was taken out for HPLC analysis.

2.7. KGN release measurement

Micelle (1 mL) solution was sealed in a dialysis bag with a molecular weight cut off at 3500 Da, and the dialysis bag was immersed in 39 mL PBS and incubated in 37 °C. At regular intervals, a 200 μL of liquid outside the bag was taken out for HPLC analysis.

2.8. Cell culture

Human ADSCs was provided by Cyagen Biosciences (HUXMD-01001; Guangzhou, China). Four tubes of primary human ADSCs cells, from the lipoaspirate of different donors, were obtained. The medium from Cyagen Biosciences (HUXMD-90011; Guangzhou, China, Table S2) was used to culture human ADSCs in a humidified incubator at 37 °C with 5% CO2. The culture medium replacement time was about 3 days. The subsequent experiments used the human ADSCs at passages 2–4. The basal differentiation media contained Dulbecco's Modified Eagle Medium (DMEM) supplemented with 10% fetal bovine serum, 2 mM L-glutamine, and 1% penicillin–streptomycin solution (Table S2). The experimental condition of human ADSCs pellets was conducted as follows: A total of 3 × 10^5 human ADSCs were placed in a 15 mL polypropylene tube, and centrifuged at 500×g for 5 min. The pellets were cultured at 37 °C with 5% CO_2 in 500 μL of differentiation medium supplemented with 1% insulin-transferrin-selenium supplement for 21 days. The pellets were fixed in 4% paraformaldehyde, embedded in O.C.T. compound, and cut into 12 μm sections. Then, nucleus pulposus differentiation was assessed by Safranin O staining and fluorescence microscopy observation.

2.9. H_2O_2-induced human ADSCs and treatment

Five groups were prepared: the human ADSCs were cultured with or without APO, KGN, and PAKM. H_2O_2 (0.4 mmol/L) were added to each group for 24 h. The groups were divided into (1) Control, (2) H_2O_2, (3) APO + H_2O_2, (4) KGN + H_2O_2, and (5) PAKM + H_2O_2. The micelle were filtered and prepared for further study.

2.10. Cellular esterase evaluation

Human ADSCs were incubated with H_2O_2 (0.4 mmol/L) overnight. Fluorescein diacetate (FDA) (Sigma-Aldrich) was dissolved with DMSO at 10 mg/mL as a storage solution, and then diluted it to 1 mg/mL with PBS as a working solution. Finally, cells were cultured with 5 μg/mL FDA in medium for 30 min before cellular esterase evaluation. The image was taken using fluorescence microscope (Leica).

2.11. Cell viability and apoptosis evaluation

CCK-8 kit (Beyotime, China)was used to test the cytotoxicity and proliferation of cells cultured with APO, KGN, and PAKM. The live/dead viability assay kit (Us everbright, China) was used to conduct Live/dead assays. Human ADSCs were incubated with fluorescein diacetate (5 μM)/propidium iodide (20 μM) at 37 °C in the dark for 5 min. The fluorescent image was taken using fluorescence microscope (Leica). Annexin V-FITC/PI Apoptosis Detection Kit (Solarbio, China) was used to measure the cell apoptosis, and then analyzed by the flow cytometer (BD Biosciences, USA).

2.12. Intracellular ROS detection

After treatment with or without H_2O_2 for 24h, human ADSCs cultured with APO, KGN, and PAKM were incubated with 20 μM dichloro-dihydro-fluorescein diacetate (DCFH-DA) at 37 °C for 0.5 h in the dark. Then cells were washed three times with PBS. The intracellular ROS level was measured by fluorescence microscope (Leica).

2.13. Assessment of autophagy

For assessment of autophagy, the secretion of LC3 II was observed by immunofluorescence. The samples were fixed with 4% formalin for 20 min, and then permeabilized with 0.3%Triton X-100 (W/V) in PBS for 30 min. After blockage by 5% BSA for 15 min, the primary antibody LC3 II (1:200 dilution, Abcam, USA) was added, and incubated at 4 °C over night, followed by the incubation of the secondary antibody Alexa Fluor 647-labeled Goat Anti-Rabbit IgG (1:500 dilution, Beyotime, China) for 12 h. The images were captured by an fluorescence microscope (Leica). The dots of LC3 II were counted by image J software.

2.14. qRT-PCR assessment

RNAiso reagent (TaKaRa Bio,Japan) was used to isolate total RNA. Reverse transcription was conducted by a PrimeScript RT reagent kit (TaKaRa, Bio, Japan). StepOnePlus Real-time PCR System (Applied Biosystems, CA, USA) and a SYBR® Premix Ex TaqTM kit (TaKaRa Bio, Japan) were used to conduct qRT-PCR. We chose 18s rRNA as the Housekeeping gene. $2^{-\triangle\triangle Ct}$ method was used to calculate the result. Sangon Biotech (Shanghai, China) provided all the primers used in this study. Table 1 listed all the primers sequences.

2.15. Western blot assessment

Human ADSCs were cultured with APO, KGN, and PAKM. RIPA lysis buffer including a protease inhibitor cocktail (Sigma-Aldrich) was used to lyse the cells for 30 min, and vortexed every 10 min. Then, the solution was centrifuged at 12,500 g at 4 °C for 15 min. The BCA protein

Table 1
Primers used in quantitative RT-PCR.

Gene	Forward primer (5′–3′)	Reverse primer (5′–3′)
18S	CGCCGCTAGAGGTGAAATTC	TTGGCAAATGCTTTCGCTC
COX2	TCCTCAGGCTTGGGTCTTGTT	TTCAGGTCACCTTGGTAGGATTTG
MMP13	ACTGAGAGGCTCCGAGAAATG	GAACCCCGCATCTTGGCTT
SOD	GGTGGGCCAAAGGATGAAGAG	CCACAAGCCAAACGACTTCC
KEAP1	CTGGAGGATCATACCAAGCAGG	GGATACCCTCAATGGACACCAC
NRF2	TCAGCGACGGAAAGAGTATGA	CCACTGGTTTCTGACTGGATGT
P62	GCACCCCAATGTGATCTGC	CGCTACACAAGTCGTAGTCTGG

assay kit (Pierce, Waltham, MA, USA) was used to quantify the protein in the supernatant. SDS-PAGE was used to separate protein at 80 V for 1.5 h. Then protein was transferred onto 2.2 μm polyvinylidene fluoride membranes (Millipore) at 250 mA for 2 h. 5% bovine serum albumin (Sigma-Aldrich) was used to block the membranes at room temperature for 1 h. Then the membranes were treated with the following primary antibodies at 4 °C overnight: ACAN (1:1000, Abcam), COL2 (1:1000; Abcam), SOX9 (1:1000, Abcam), KRT19 (1:1000, Cell Signaling Technology), COX2 (1:1000, Abcam), MMP-13 (1:1000, Abcam), and GAPDH (1:1000; Santa Cruz, USA). Finally, the membranes were treated with horseradish peroxidase (HRP)-conjugated secondary antibodies (Cell Signaling Technology) at room temperature for 1 h. An enhanced chemiluminescence kit (Millipore) was used to detect the immunoreactivity.

2.16. Animal surgery

The Sprague–Dawley rats were purchased from the Shanghai Laboratory Animal Center of the Chinese Academy of Sciences. The study was approved by the local authorities (the Second Affiliated Hospital of Zhejiang University School of Medicine, China). Our previous study described the surgical procedure used in this study [27]. The rats were intraperitoneally injected with 1% pentobarbital sodium (Sigma Aldrich, St. Louis, MO, 0.4 mL/kg). Palpation was used to determine the intervertebral discs of coccygeal (Co) vertebrae Co7/Co8, Co8/Co9, and Co9/Co10. Then, we inserted a 20-G sterile needle with a handmade stopper into the middle of the disc for a depth of 5 mm, rotated 360°, and held for 30 s. 80 male rats with an average weight of 270 g at the day of surgery were randomly divided into four groups: The control group (NC) (without needle puncture); The degeneration group (DC) (with needle puncture and PBS injection); The PAKM (with needle puncture and PAKM injection); And the PAKM with human ADSCs group (PAKMA) (with needle puncture and PAKM with human ADSCs injection). 2 μl of material was injected into the NP of Co7/Co8, Co8/Co9, and Co9/Co10 by a 31-G needle. Fifteen-independent IVDs (5 rats) of different groups obtained at 0, 4, 8, and 16 weeks for futher experiment.

2.17. Disc height evaluation

Molybdenum target (GEMammography DMR Bucky 18 × 24, GE Healthcare, Little Chalfont, UK) was used to evaluate disc height at 0 and 16 weeks. We put the rats in the prone position, and straightened the tail. A computed radiographic plate system (AGFA Diagnostic Center Compact Plus, AGFA HealthCare, Mortsel, Belgium) was used to obtain the digital images. The disc height was evaluated by National Institutes of Health software.

2.18. Magnetic resonance imaging (MRI) evaluation

A 3.0 T MRI scanner (Signa Excite, General Electric Medical Systems, Little Chalfont, UK) was used to assessed the IVDD of the rat tail. The structure of NP was assessed by T2-weighted sections in a sagittal plane at 0 and 16 weeks after injection. We put the rats in the prone position, and straightened the tail. The MRI scanner parameters were set as follow: spin echo repetition time, 2275 ms; echo time, 80 ms; number of excitations, 8; field of view, 5 cm; slice thickness, 1.5 mm; no phase wrap. The image slices was analyzed by a GE ADW4.2 workstation. Finally, the alteration of NP was evaluated by the Pfirrmann grading system [28].

2.19. Histological evaluation

The rats were killed at the indicated time points after micelle injection, and the intervertebral discs were fixed in 10% formalin, and sliced for histologic evaluation. The graded alcohol series and paraffin were used to dehydrate, and embed the samples respectively. The slice thickness of intervertebral disc was 5 μm sections. Safranin O-fast green (S–O) or hematoxylin and eosin (H&E) staining were conducted. Two observers in a blinded fashion assessed the cellularity and morphology. The grading scale was used as previously reported [29,30].

2.20. Immunohistochemistry evaluation

For immunohistochemistry evaluation, intervertebral disc sections were deparaffinized in xylene, and then hydrated with gradient increased alcohol. The sections were treated with 3% H_2O_2 for 15 min and 10% goat serum for 15 min. Then the samples were treated with mouse monoclonal antibodies against type II collagen at 4 °C overnight. The samples were incubated with biotin labeled secondary antibody at 37 °C for 30 min, after washing five times with PBS. The SABC method was used to detect the staining. Images were recorded by a DP70 CCD camera (Olympus) coupled with an AX-70 microscope (Olympus).

2.21. Statistics

The data is presented as mean ± S.D. The one-way ANOVA and Tukey's post-hoc test or nonparametric test were used to calculate the statistical significance of the differences between the groups. Experiments were repeated at least three times with identical results. All statistical analysis was performed in SPSS software 22.0 (SPSS Inc., Chicago, USA). $P < 0.05$ was determined as statistical significance.

3. Results

3.1. Preparation and characterization of the micelles

An amphiphilic copolymer PEG-PAPO was synthesized, which could self-assemble into a nanosized micelle and load KGN. First, the monomer HAPO was synthesized by conjugating APO with HEMA via an ester bond. PEG-PAPO was synthesized by Reversible Addition-Fragmentation Chain Transfer Polymerization (RAFT) of HAPO with PEG-PETTC as the chain transfer agent (Fig. 1A). The formation of PEG-PAPO was confirmed by ^{1}H nuclear magnetic resonance (^{1}H NMR) (Fig. 1B), which showed that average 16 APOs were linked to a polymer chain, whose molecular weight was estimated to be ca.10 kDa. Gel permeation chromatography (GPC) of PEG-PETTC and PEG-PAPO indicated the copolymer was successfully synthesized with an Mn of 33 kDa and a polydispersity index (PDI) of 1.17 (Fig. 1C).

PEG-PAPO could assemble into micelles in aqueous solution, and KGN could be effectively loaded into the micelles, forming PAKM, because of the hydrophobic properties of APO and KGN and the π-π stacking interactions between them. The loading content and efficiency tested by HPLC were 3.7% and 38.8%, respectively. PAKM was characterized by dynamic light scattering (DLS). The average-volume hydrodynamic diameter was 49.8 nm with a PDI of 0.13, and zeta potential of −34.2 mV (Fig. 1D). APO was gradually released from PAKM under the presence of 120 U/mL esterase, while APO was seldomly released from PAKM in the absence of esterase (Fig. 1E). However, 90% of the loaded KGN was released from the micelle after 4h incubation in PBS (Fig. 1F). The above results confirmed the successful drug-loading of the micelles and the esterase-responsive APO release property.

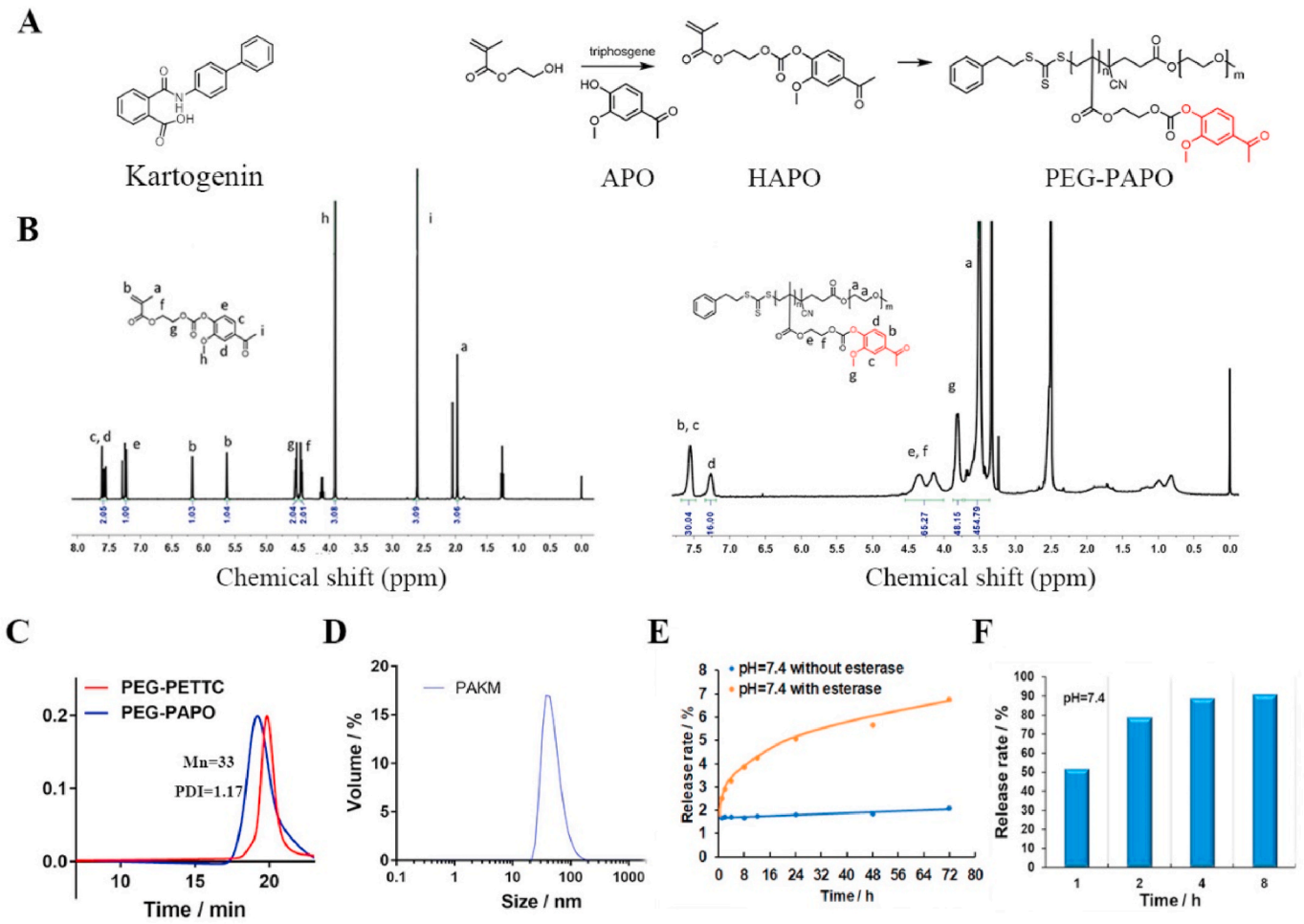

Fig. 1. Synthesis and characterization of an esterase-responsive micelle polymer (PAKM) for intervertebral disc degeneration stem cell therapy. (A) The synthesis protocol for PEG-PAPO. (B) ^{1}H NMR spectrum (400 MHz, DMSO) of the HAPO and PEG-PAPO. (C) GPC traces of PEG-PETTC, PEG-PAPO. (D) Size distribution of PAKM measured by the DLS. (E) APO and (F) KGN was released from the micelle into Dulbecco's phosphate buffered saline at 37 °C.

3.2. Esterase-responsiveness of PAKM

Esterase activity in human ADSCs (Fig. 2A) was demonstrated by fluorescein diacetate (FDA), using methods described in our previous research [31]. Our results demonstrated that esterase activity increased in human ADSCs after oxidative stimulation by H_2O_2 compared to the control group (Fig. 2B). The increased esterase activity favored the esterase-responsive APO release in human ADSCs.

3.3. Effect of PAKM on the cell viability of H2O2-stimulated human ADSCs

For further investigation, we evaluated the biological effects of De-PAKM (degradation products of PAKM acquired using esterase) *in vitro*. Testing for possible cytotoxicity of De-PAKM in human ADSCs, we found that cell numbers did not decrease after incubation with De-PAKM (Maximally release KGN from 10 to 1000 nM) after 1, 7, and 14 days, demonstrating good biocompatibility of De-PAKM with stem cells (Fig. 2C). Viability of human ADSCs was analyzed using a Cell Counting Kit-8 (CCK-8) assay. After H_2O_2 exposure (12 h), the viability of human ADSCs cultured with APO, KGN, and De-PAKM was investigated (Fig. 2D). The viability levels of human ADSCs were 54.1% in H_2O_2-treated group; 68.8% in the KGN + H_2O_2 group; 77.8% in the APO + H_2O_2 group and 89.6% in the De-PAKM + H_2O_2 group. The data provide clear evidence that De-PAKM is an effective tool for improving cell viability under H_2O_2-induced oxidative stress.

To further confirm these results, ratios of live/dead cells were assessed by fluorescence cell imaging. (Fig. 2E). In these assays, H_2O_2 treatment increased the numbers of dead cells (red), and reduced the numbers of live cells (green). APO-, KGN-, and De-PAKM-treated cells showed higher percentage of live cells from all cells, of 91.6%, 92.4%, and 97.5%, respectively, under the oxidative stress, than cells treated with H_2O_2 alone (78.8%) (Fig. 2F).

Apoptotic human ADSCs levels were also evaluated by flow cytometry (Fig. 2G). De-PAKM treatment consistently reduced H_2O_2-induced apoptosis. In contrast, Cell apoptosis rate of human ADSCs was 15.68% when treated with H_2O_2. Apoptosis rate reduced to 5.66% with De-PAKM treatment, 11.88% with APO treatment and 14.09% with KGN. Therefore, De-PAKM is the effective agent in protecting human ADSCs from oxidative stress.

3.4. Inhibition of inflammatory factor and catabolic gene expression by PAKM

A specific catabolic gene (matrix metalloproteinase-13, MMP-13) is essential for IVDD pathogenesis. MMP-13 is the major catabolic factor in ECM metabolism [32–34]. The inflammation-associated gene (COX-2) in human ADSCs was also studied [35]. To investigate ECM degradation in IVDD, we used protein assays to evaluate MMP-13 and COX2 expression in H_2O_2 -stimulated human ADSCs treated with De-PAKM (Fg. 3A, B). H_2O_2 stimulation increased the expression of MMP-13 and COX-2, but this increase was reduced by KGN, APO, and De-PAKM. In

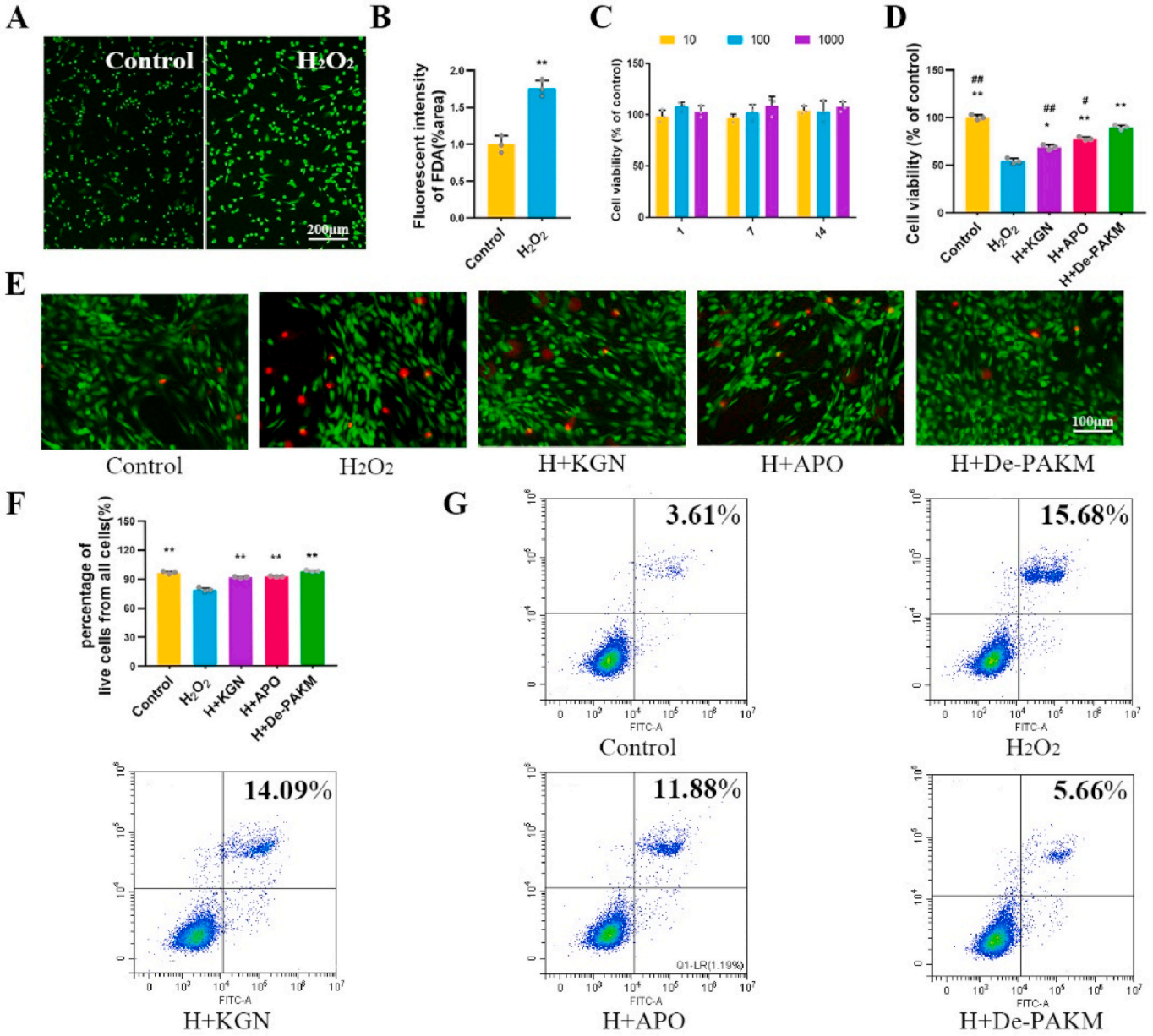

Fig. 2. PAKM reduced cell apoptosis and maintained cell viability after inflammatory stimulation. (A, B) Esterase activity of human ADSCs with or without H_2O_2 stimulation, was determined using fluorescein diacetate, and observed under a fluorescence microscope (Scale bar = 200 μm); (C) Cytotoxicity of PAKM at different concentrations on human ADSCs at different time points. (D) Cell viability of cells cultured with KGN and De-PAKM. (E) Fluorescence image of live (green) and dead (red) cells with or without H_2O_2 exposure. (Scale bar = 100 μm) (F) Quantification of percentage of live cells from all cells. (G) Detection of cell apoptosis by flow cytometry after treatment with or without H_2O_2. Data represent the mean ± SD; *p < 0.05 and **p < 0.01 vs the H_2O_2 group; #p < 0.05 and ##p < 0.01 vs the De-PAKM group. Sample numbers N = 3. (For interpretation of the references to colour in this figure legend, the reader is referred to the Web version of this article.)

short, De-PAKM shows the greatest ability to resist oxidative stress-induced ECM degradation. qRT-PCR analysis also corroborated this finding (Fig. 3C). These results indicated that H_2O_2-induced inflammation in human ADSCs was significantly suppressed by De-PAKM.

3.5. PAKM suppressed H_2O_2-induced oxidative stress

The antioxidant activity of PAKM was assessed by qRT-PCR analysis. We compared expression of the antioxidant enzyme SOD (Fig. 3C) in H_2O_2-treated human ADSCs cultured with APO and KGN, to those cultured with De-PAKM; in these conditions, De-PAKM cells showed the greatest increase in SOD expression. We also evaluated H_2O_2-induced intracellular ROS production by immunofluorescence analysis, using a DCFH-DA probe (Fig. 3E) that can freely cross plasma membranes. Intracellular esterase hydrolyses DCFH-DA, and generates dichlorofluorescin (DCFH), intracellular ROS oxidizes DCFH and produces fluorescent dichlorofluorescein (DCF). Thus, this probe is a sensitive indicator of ROS, demonstrating that H_2O_2 generally induces an increase in intracellular ROS in human ADSCs. These results indicate that De-PAKM can enhance the ability of human ADSCs to resist oxidative stress (Fig. 3D).

3.6. The differentiation efficiency of human ADSCs in the NP with PAKM

The matrix-synthesis ability of human ADSCs is demonstrated by the gene expression and protein levels of Aggrecan and COL2A1, all of which were higher in the PAKM group than the control, H_2O_2, and

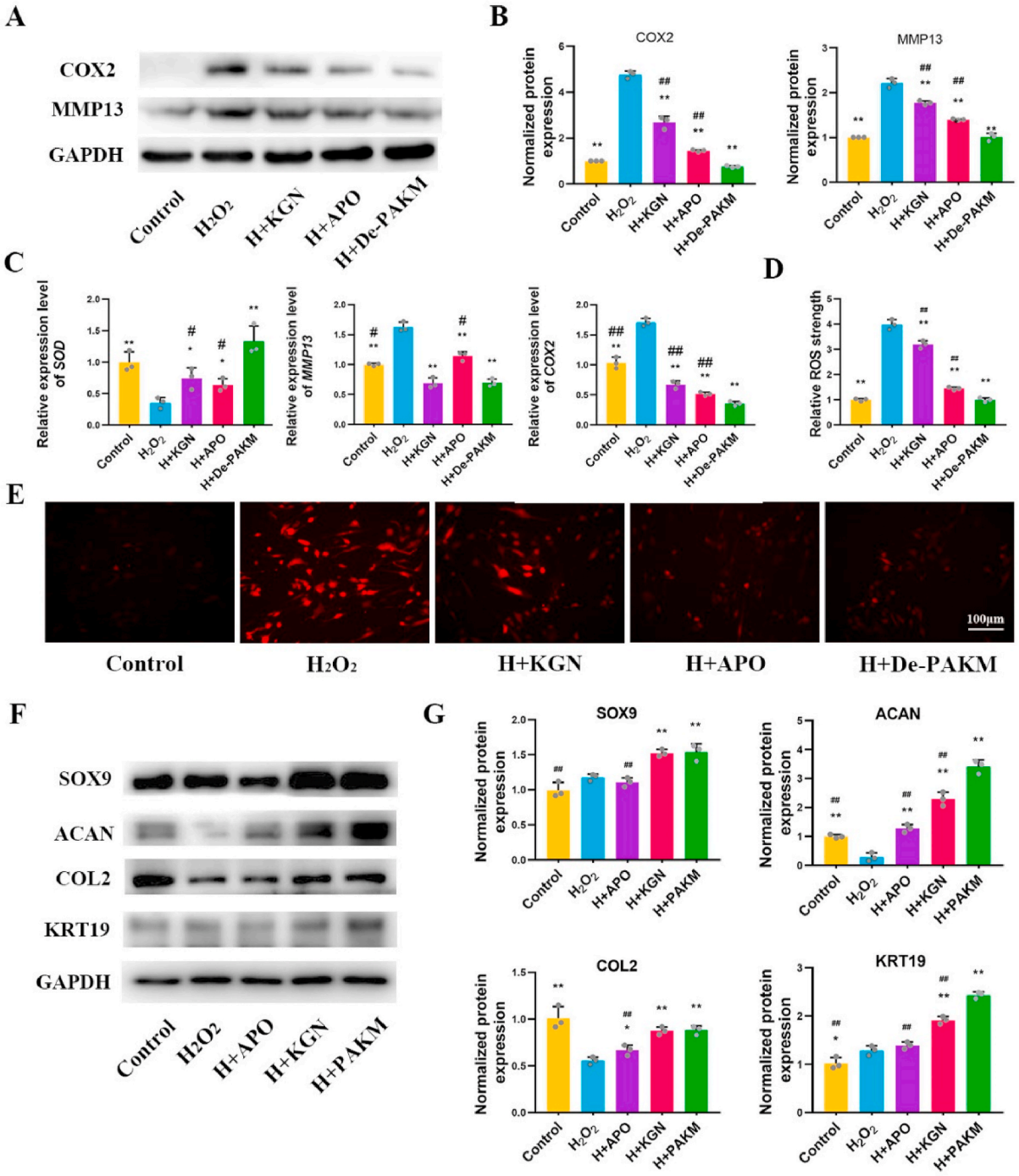

Fig. 3. Suppression of H_2O_2-induced oxidative stress and extracellular matrix release from human ADSCs. (A, B) Western blot detection for MMP-13 and COX2 in human ADSCs cultured with De-PAKM. (C). qRT-PCR detection of inflammatory factors MMP-13, COX2 and antioxidant factors SOD in human ADSCs cultured with De-PAKM. (D) Quantification of relative ROS strength. (E) Intracellular ROS detection with dichloro-dihydro-fluorescein diacetate (DCFH-DA) obtained by immunofluorescence staining. (F) Protein expression levels of SOX9, Aggrecan, COL2, and KRT19 were measured on day 21. (G) Representative Western blot images and quantification of expression levels are shown. GAPDH served as a loading control. Data represent the mean ± SD; *p < 0.05 and **p < 0.01 vs the H2O2 group; #p < 0.05 and ##p < 0.01 vs the De-PAKM group. Sample numbers N = 3.

H_2O_2+APO groups on day 21 (Fig. 3F and G). Previous studies reported that positive relationship existed between SOX9 expression and maintenance of a healthy ECM [36]. PAKM group also show highest expression level of transcription factor SOX9. KRT19 exhibited a high nucleus pulposus: annulus fibrosus ratio and a high nucleus pulposus: articular cartilage ratio, thus making this a perfect marker for NP cells [37]. Human ADSCs cultured with PAKM shows higher KRT19 levels compared to either the KGN or APO treatment group. Safranin-O staining and fluorescence microscopy observation of COL2A1 indicated that PAKM significantly induces differentiation of human ADSCs into an NP-like phenotype (Fig. S1). All these data demonstrate that PAKM has a strong ability to inhibit ECM degradation and to induce nucleus pulposus differentiation of human ADSCs under oxidative stress.

3.7. PAKM activated autophagy

Autophagy plays a crucial role in removal of dysfunctional organelles and protein aggregates in maintaining stem-cell homeostasis, and can assist cells in resisting excessive oxidative stress in IVDD [38–40]. The presence of autophagosomes is an indication of autophagy. We detected the presence of autophagosomes by immunofluorescence (Fig. 4C) of LC3 II. There are fewer autophagic vacuoles in the absence of H_2O_2 stimulation. After exposure to H_2O_2 for 24 h, human ADSCs cultured with De-PAKM shows more dots of LC3 II, thus indicating the presence of autophagosomes, compared to that of cells cultured with APO and KGN group (Fig. 4D). These results show that De-PAKM activated autophagy in human ADSCs more effectively than other treatments. We also evaluated protein and gene expression levels of the autophagy markers KEAP1, LC3 II, and P62 (Fig. 4A, B, E). In contrast to APO and KGN treatment, the LC3 II expression levels were significantly up-regulated in De-PAKM-treated cells. Notably, KEAP1 and P62 was suppressed in De-PAKM group. The KEAP1-NRF2 system plays a key role in the adjustment of redox homeostasis [41], and the NRF2 signaling pathway is negatively regulated by KEAP1 in autophagy under oxidative stress. Therefore, our results suggest that De-PAKM suppressed H_2O_2-induced oxidative stress in human ADSCs by activating autophagy.

3.8. Disc height assessment in different groups by X-ray and MRI analysis

Intervertebral disc height was evaluated by X-ray analysis to assess the treatment effects of PAKM *in vivo* (Fig. 5A and B). The disc height index (DHI%) value of the control, disc degeneration, PAKM, and PAKMA group were significantly decreased at all time points compared with that of the control group. The DHI% values of the degeneration, PAKM, and PAKMA groups showed no obvious differences at week 0; however, at16 weeks, the PAKMA group showed much stronger treatment effects than that the PAKM and degeneration group ($p < 0.01$) (Fig. 5C). MRI is an efficient method for evaluating the water content and composition of intervertebral discs (Fig. 5D). According to the Pfirrmann grading system [28], the severity of IVDD in the four groups was totally different at 16 weeks after treatment ($\chi^2 = 51.33$, $P < 0.001$) (Fig. 5E). At 16 weeks, PAKMA group showed four IVDs graded II, two IVDs graded III. Meanwhile, the degenerative group without treatment showed the most severe degeneration (grade IV = 1, grade V = 5 at 16 weeks).

3.9. Histological and immunohistochemical evaluation of intervertebral discs

The control group showed complete NP structure and collagen arrangement in the annulus fibrosus (Fig. 6A). In the degeneration group, however, intervertebral disc structure was destroyed. The contents of the intervertebral disc were decreased with disorganized hypocellular fibrocartilaginous tissue. Although discs in the PAKMA group were degraded to some extent, the PAKMA group exhibited more complete disc morphology than the PAKM and degeneration groups. The

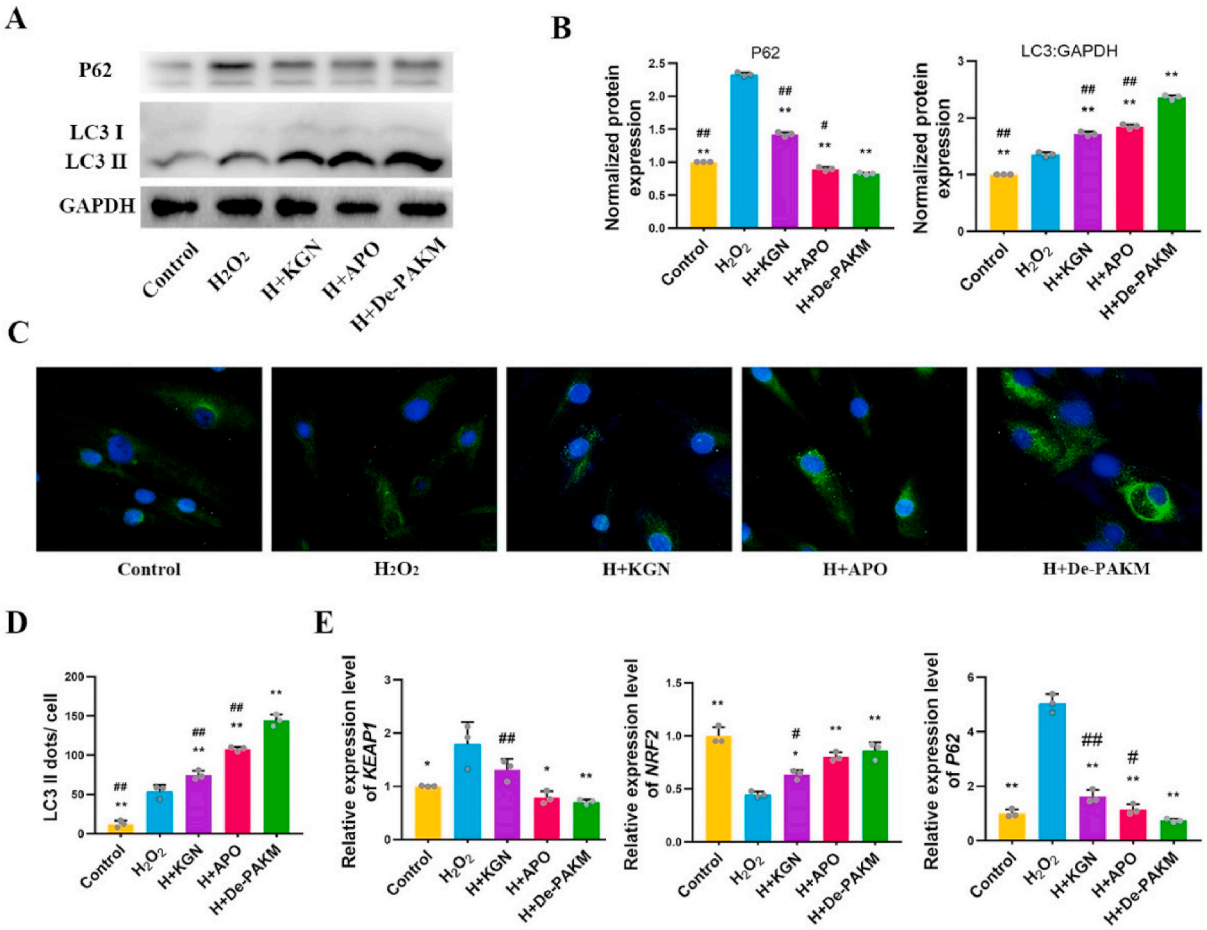

Fig. 4. Autophagy activation by De-PAKM protect human ADSCs from H_2O_2-induced oxidative stress. (A, B) Western blot detection for P62 and LC3II in human ADSCs cultured with PAKM. (C) Fluorescence microscopy observation of LC3 (green) in human ADSCs after treatment with H_2O_2. (D) Quantification of LC3IIdots/cell. (E) qRT-PCR detection of expression levels of autophagy markers KEAP1, NRF2, and P62. Data represent the mean ± SD; *$p < 0.05$ and **$p < 0.01$ vs the H2O2 group; #$p < 0.05$ and ##$p < 0.01$ vs the De-PAKM group. Sample numbers N = 3. (For interpretation of the references to colour in this figure legend, the reader is referred to the Web version of this article.)

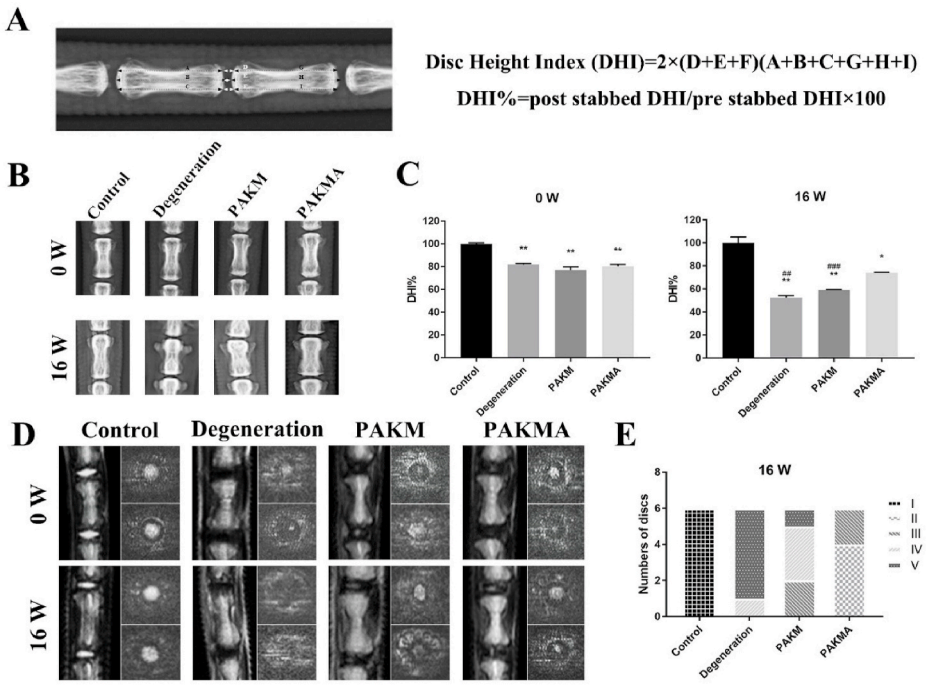

Fig. 5. Disc height indices were measured from digitized radiographs using NIH software (A, B) Representative radiographs of the rat Co7/Co8 and Co8/Co9 were obtained from the four groups at 4 and 16 weeks after injection. (C) Disc height changes of the four groups were measured at different time points. (D) Representative T2 MRI scans of different groups were obtained at 0 and 16 weeks. (E) The Pfirrmann grading system of different experimental groups were used to quantify the structure, distinction of nucleus and annulus fibrosus, signal intensity, and height of intervertebral disc ($\chi 2 = 51.33$, $P < 0.001$). PAKM (with needle puncture and PAKM injection); PAKM with human ADSCs group (PAKMA) (with needle puncture and PAKM with human ADSCs injection. Data represent the mean ± SD; *p < 0.05 and **p < 0.01 vs the control group; ##p < 0.01 and ###p < 0.001 vs the PAKMA group. Sample numbers N = 6.

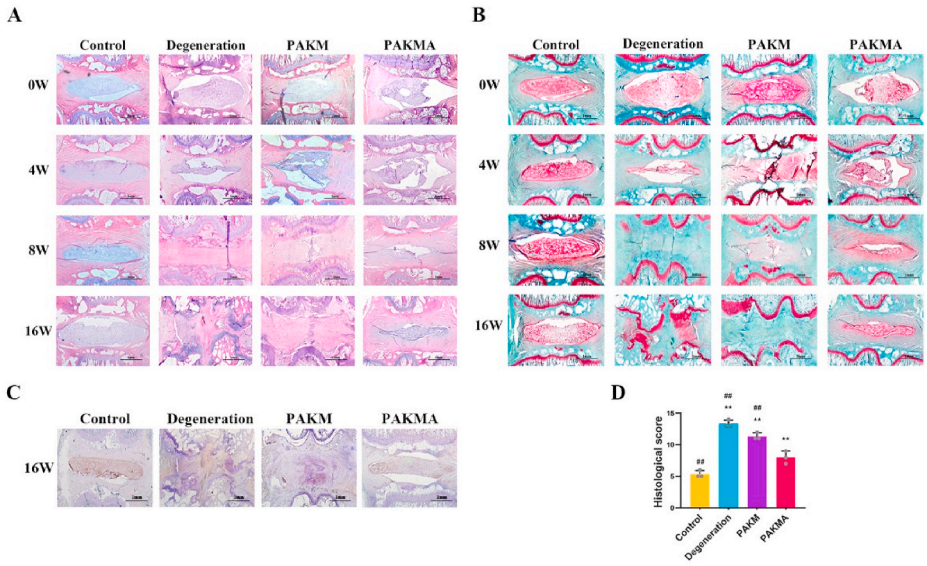

Fig. 6. (A, B) Representative images of H&E and SO staining of different groups obtained at 0, 4, 8, and 16 weeks after injection. (C) Immunohistochemical detection of type II collagen in the intervertebral disc from different groups at 16 weeks after injection. (D) A histogram showing the histological scores of four groups evaluated at 16 weeks after injection. PAKM (with needle puncture and PAKM injection); PAKM with human ADSCs group (PAKMA) (with needle puncture and PAKM with human ADSCs injection. Data represent the mean ± SD; *p < 0.05 and **p < 0.01 vs the control group; #p < 0.05 and ##p < 0.01 vs the PAKMA group. Sample numbers N = 6.

PAKMA group, for instance, showed no evidence of incursion of blood vessels within the discs. Safranin-O staining demonstrated a decrease in proteoglycans in the degeneration, PAKM, and PAKMA groups. PAKMA showed less disc degeneration than the PAKM group (Fig. 6B), and the histologic scores of the PAKMA group, evaluated by the methods described in Table S1 [9], was significantly lower than the PAKM and degeneration groups (Fig. 6D). The PAKM group showed evidence of partial damage repair, and the PAKMA group showed evidence of marked improvement. The control group contained well-organized type II collagen, proved by Immunohistochemical staining (Fig. 6C). At 16 weeks, type II collagen staining in the degeneration and PAKM groups was lower than that in the PAKMA group, proving a lack of disc structure in the first two groups, and a more normal structure in PAKMA group.

4. Discussion

In this study, we have proposed a novel strategy for treatment of IVDD. The mechanism and effectiveness of the proposed therapy was carefully validated both *in vitro* (human ADSCs) and *in vivo* (a rat IVDD model). As the core of our strategy for IVDD treatment, we designed an APO-based amphiphilic micelle, which was readily synthesized by linking APO monomer via an esterase-responsive phenolic ester bond and loading lipophilic KGN in the core of the micelle. Our work demonstrates that PAKM could protect human ADSCs from oxidative stress, and promote human ADSCs differentiation into an NP-like phenotype.

Stem cell transplantation therapy is a promising strategy for IVDD treatment. Human ADSCs are multipotent cells characterized by their ability to differentiate into adipocytes, chondrocytes, and osteoblasts [42]. Previous studies have demonstrated the beneficial effect of

mesenchymal stem cells on intervertebral disc degeneration [43–45]. But there are still many problems between the microenvironment and transplanted cells. Although some ROS serve as signaling molecules in cells, excessive oxidative and inflammation production is harmful and has been implicated in progression of IVDD [46]. ROS production and nonspecific inflammation generated during the IVDD pathological process have been demonstrated in leading to loss of transplanted stem cells. In conclusion, cellular damage and dysfunction occur with high ROS levels. Therefore, Attenuation of ROS-induced cell apoptosis and promotion of cell differentiation were essential for getting greater clinical success in cell transplantation therapy [47,48].

The anti-aging and anti-apoptotic capability of APO in mesenchymal stem cells has been reported on intracerebral hemorrhage and myocardial infarction [23,24]. Our study first confirmed that APO stimulated the proliferation and survival rate of human ADSCs on IVDD. Secondly, KGN was reported to effectively repair the degeneration of intervertebral disc. Yao et al. demonstrated the effects of KGN on the attenuated nucleus pulposus cell degeneration induced by interleukin-1β and tumor necrosis factor-α [49]. Zhu et al. shown developed the KGN-conjugated chitosan–hyaluronic acid hydrogel, which promote human ADSCs proliferation and nucleus pulposus differentiation [25]. Although above studies shown regenerative effects of IVDD to a certain extent, excessive oxidative stress in the lesion site still causes hyper-peroxidation, protein carbonylation and DNA damage to transplanted human ADSCs. Importantly, we have herein demonstrated that the antioxidant PAKM increases human ADSCs viability by reducing inflammation factors (COX2, MMP-13), suppressing ROS, and activating antioxidant enzymes (SOD). In addition, APO and KGN released from our micelles stimulate autophagy via KEAP1-NRF2 axis. P62 phosphorylates and interacts with the NRF2-binding site of KEAP1, inhibiting KEAP1-NRF2 interaction, and resulting in upregulation of these genes under oxidative stress. Previous research demonstrated that KGN promotes silent information regulator type 1 (SIRT1) expression to enhance the intracellular antioxidant properties of mesenchymal stem cells [50]. There may thus exist a positive feedback loop between SIRT1 and KEAP1/NRF2 anti-oxidative pathway to suppress ROS overproduction [51]. The positive feedback loop discussed above may explain the anti-oxidative ability of KGN. Furthermore, histological and immunohistochemical data confirm that the PAKM micelles effectively suppress IVDD progression and nucleus pulposus degradation, and this is the main purpose of our study to protect human ADSCs from oxidative stress.

KRT19 is specifically expressed in cells with an NP-like phenotype. Meanwhile, the COL2, Aggrecan genes can be used for evaluating the extracellular matrix releasing ability of differentiated cells [37]. Therefore, the differentiation and extracellular matrix releasing ability of human ADSCs can be effectively evaluated using these genes in this study.

PAKM, combined with human ADSCs injection, has been shown to be a minimally invasive strategy for nucleus pulposus repair that is applicable to IVDD treatment. However, the sustained release profile of micelles has this far been tested only *in vitro*. Further assessment is needed to measure the quantity of APO and KGN content in the discs. Our previous studies described a tail disc degeneration model generated via acupuncture [27]. This animal model facilitates injection of micelles into the injury area, and histologic and radiographic signs of disc degeneration can be successfully monitored. In IVDD, disc height, water content, ECM, and NP cell number all decrease [3]. Our results show that injection of PAKM with human ADSCs yields better treatment results than in the degeneration and PAKM groups. In the degeneration group, intervertebral discs structures were obviously destroyed. Our study evaluated the morphology of the AF and NP were evaluated by histological score. The histological score of the PAKMA group was significantly lower than that of either the PAKM or the degeneration group. Although IVDD degeneration was indeed attenuated in the PAKMA group, its histological score was still higher than that in control group. In conclusion, injection of PAKM has no obvious activity on alleviating IVDD. Though the PAKMA partially alleviated IVDD, it presented a better treatment activity on alleviating IVDD than the PAKM group. This result may be due to the influence of APO and KGN on human ADSCs, which affect scavenging ROS, reducing cell apoptosis and maintaining the differentiation potential of human ADSCs.

Although histology and imaging data indicate that the PAKM micelles injected with human ADSCs provided better treatment effects than the other groups, even in this group, normal intervertebral disc capabilities were not recovered completely. Several studies shown that, although high ROS levels cause cellular damage and dysfunction, a low basal level of ROS is necessary to maintain normal cellular proliferation, differentiation, and survival. Further investigation is needed to fully clarify the necessary balance between ROS and stem cells. Our work has shown that dramatically increased ROS production leads to loss of transplanted mesenchymal stem cells from this site. The injectable PAKM micelle is an effect tool to maximize the biological effects and survival rate of stem cells. Finally, micro CT, flexibility tests, and axial compression tests are also reliable strategies for evaluating the effect of biological therapies.

5. Conclusions

In our study, an injectable esterase-responsive KGN load PAPO micelle PAKM was developed to codelivery APO and KGN into intervertebral discs. The results demonstrate the biosafety of PAKM, and its ability to stimulate differentiation of human ADSCs and to protect cells by suppressing oxidative stress. As a result, PAKM combined with human ADSCs could alleviate IVDD *in vivo*, providing a novel strategy in developing biological therapies for IVDD.

CRediT authorship contribution statement

Chao Yu: Writing – original draft, Writing – review & editing. **Dongdong Li:** Writing – original draft, Writing – review & editing. **Chenggui Wang:** Writing – review & editing. **Kaishun Xia:** Writing – review & editing. **Jingkai Wang:** Writing – review & editing. **Xiaopeng Zhou:** Writing – review & editing. **Liwei Ying:** Writing – review & editing. **Jiawei Shu:** Writing – review & editing. **Xianpeng Huang:** Writing – review & editing. **Haibin Xu:** Writing – review & editing. **Bin Han:** Formal analysis, Writing – review & editing. **Qixin Chen:** Writing – review & editing, Formal analysis. **Fangcai Li:** Writing – review & editing, Formal analysis. **Jianbin Tang:** Writing – review & editing, Formal analysis. **Chengzhen Liang:** Writing – review & editing. **Nigel Slater:** Writing – review & editing, Formal analysis.

Declaration of competing interest

The authors declare no competing financial interest.

Acknowledgements

This study was supported by grants from the Nature Science Foundation of Zhejiang Province (Y20H060063, LY19H060005, LQ18H060003, LR18E030002, LY18H060004), the Medical and Health Innovation Talent Support Program of Zhejiang Province (2020RC011), the National Natural Science Foundation of China (NO.82072465, NO.81772379, NO.81972096, NO.81902238, NO.21774109, NO.51973188, NO.51522304), the Health Foundation of Zhejiang Province (2018KY092, WKJ-ZJ-1903), the China Postdoctoral Science Foundation (2017M612011), the Zhejiang University Education Foundation Global Partnership Fund, a project supported by the Scientific Research Fund of Zhejiang Provincial Education Department (Y201941476 and Y201941491), Zhejiang Undergraduate Talent Project (grant no. 2020R401212) and the Scientific Research Fund of Zhejiang Provincial Education Department (Y201941476).

Appendix A. Supplementary data

Supplementary data to this article can be found online at https://doi.org/10.1016/j.bioactmat.2021.03.018.

References

[1] B.I. Martin, R.A. Deyo, S.K. Mirza, et al., Expenditures and health status among adults with back and neck problems, J. Am. Med. Assoc. 299 (6) (2008) 656–664, https://doi.org/10.1001/jama.299.6.656.

[2] J. Takatalo, J. Karppinen, J. Niinimaki, et al., Does lumbar disc degeneration on magnetic resonance imaging associate with low back symptom severity in young Finnish adults? Spine 36 (25) (2011) 2180–2189, https://doi.org/10.1097/BRS.0b013e3182077122.

[3] P.P. Raj, Intervertebral disc: anatomy-physiology-pathophysiology-treatment, Pain Pract. 8 (1) (2008) 18–44, https://doi.org/10.1111/j.1533-2500.2007.00171.x.

[4] R.D. Bowles, L.A. Setton, Biomaterials for intervertebral disc regeneration and repair, Biomaterials 129 (2017) 54–67, https://doi.org/10.1016/j.biomaterials.2017.03.013.

[5] M.D. Humzah, R.W. Soames, Human intervertebral disc: structure and function, Anat. Rec. 220 (4) (1988) 337–356, https://doi.org/10.1002/ar.1092200402.

[6] D. Sakai, G.B. Andersson, Stem cell therapy for intervertebral disc regeneration: obstacles and solutions, Nat. Rev. Rheumatol. 11 (4) (2015) 243–256, https://doi.org/10.1038/nrrheum.2015.13.

[7] A.L.A. Binch, J.C. Fitzgerald, E.A. Growney, et al., Cell-based strategies for IVD repair: clinical progress and translational obstacles, Nat. Rev. Rheumatol. (2021), https://doi.org/10.1038/s41584-020-00568-w.

[8] S.M. Richardson, G. Kalamegam, P.N. Pushparaj, et al., Mesenchymal stem cells in regenerative medicine: focus on articular cartilage and intervertebral disc regeneration, Methods 99 (2016) 69–80, https://doi.org/10.1016/j.ymeth.2015.09.015.

[9] J. Zhu, K. Xia, W. Yu, et al., Sustained release of GDF5 from a designed coacervate attenuates disc degeneration in a rat model, Acta Biomater. 86 (2019) 300–311, https://doi.org/10.1016/j.actbio.2019.01.028.

[10] C.J. Ma, X. Liu, L. Che, et al., Stem cell therapies for intervertebral disc degeneration: immune privilege reinforcement by fas/FasL regulating machinery, Curr. Stem Cell Res. Ther. 10 (4) (2015) 285–295, https://doi.org/10.2174/1574888x10666150416114027.

[11] Z.F. Lu, B.Z. Doulabi, P.I. Wuisman, et al., Influence of collagen type II and nucleus pulposus cells on aggregation and differentiation of adipose tissue-derived stem cells, J. Cell Mol. Med. 12 (6B) (2008) 2812–2822, https://doi.org/10.1111/j.1582-4934.2008.00278.x.

[12] V.Y. Leung, D. Chan, K.M. Cheung, Regeneration of intervertebral disc by mesenchymal stem cells: potentials, limitations, and future direction, Eur. Spine J. 15 (Suppl 3) (2006) S406–S413, https://doi.org/10.1007/s00586-006-0183-z.

[13] C. Liang, H. Li, Y. Tao, et al., Responses of human adipose-derived mesenchymal stem cells to chemical microenvironment of the intervertebral disc, J. Transl. Med. 10 (2012) 49, https://doi.org/10.1186/1479-5876-10-49.

[14] S. Chen, S. Liu, L. Zhao, et al., Heme oxygenase-1-mediated autophagy protects against oxidative damage in rat nucleus pulposus-derived mesenchymal stem cells, Oxid Med Cell Longev 2020 (2020) 9349762, https://doi.org/10.1155/2020/9349762.

[15] E. Gibon, L. Lu, S.B. Goodman, Aging, inflammation, stem cells, and bone healing, Stem Cell Res. Ther. 7 (2016) 44, https://doi.org/10.1186/s13287-016-0300-9.

[16] W. Wagner, P. Horn, M. Castoldi, et al., Replicative senescence of mesenchymal stem cells: a continuous and organized process, PloS One 3 (5) (2008), e2213, https://doi.org/10.1371/journal.pone.0002213.

[17] J. Stefanska, R. Pawliczak, Apocynin: molecular aptitudes, Mediat. Inflamm. 2008 (2008) 106507, https://doi.org/10.1155/2008/106507.

[18] T.S. Hiran, P.J. Moulton, J.T. Hancock, Detection of superoxide and NADPH oxidase in porcine articular chondrocytes, Free Radic. Biol. Med. 23 (5) (1997) 736–743, https://doi.org/10.1016/s0891-5849(97)00054-3.

[19] S.S. Barbieri, V. Cavalca, S. Eligini, et al., Apocynin prevents cyclooxygenase 2 expression in human monocytes through NADPH oxidase and glutathione redox-dependent mechanisms, Free Radic. Biol. Med. 37 (2) (2004) 156–165, https://doi.org/10.1016/j.freeradbiomed.2004.04.020.

[20] E.A. Peters, J.T. Hiltermann, J. Stolk, Effect of apocynin on ozone-induced airway hyperresponsiveness to methacholine in asthmatics, Free Radic. Biol. Med. 31 (11) (2001) 1442–1447, https://doi.org/10.1016/s0891-5849(01)00725-0.

[21] S. Hougee, A. Hartog, A. Sanders, et al., Oral administration of the NADPH-oxidase inhibitor apocynin partially restores diminished cartilage proteoglycan synthesis and reduces inflammation in mice, Eur. J. Pharmacol. 531 (1–3) (2006) 264–269, https://doi.org/10.1016/j.ejphar.2005.11.061.

[22] V.F. Ximenes, M.P. Kanegae, S.R. Rissato, et al., The oxidation of apocynin catalyzed by myeloperoxidase: proposal for NADPH oxidase inhibition, Arch. Biochem. Biophys. 457 (2) (2007) 134–141, https://doi.org/10.1016/j.abb.2006.11.010.

[23] S. Min, O.J. Kim, J. Bae, et al., Effect of pretreatment with the NADPH oxidase inhibitor apocynin on the therapeutic efficacy of human placenta-derived mesenchymal stem cells in intracerebral hemorrhage, Int. J. Mol. Sci. 19 (11) (2018), https://doi.org/10.3390/ijms19113679.

[24] D. Feng, L. Zhang, F. Ding, et al., Blocking Nox 2 improves mesenchymal stem cells therapy in myocardial infarction via antagonizing oxidant and promoting survival, J. Cell. Physiol. 233 (10) (2018) 7004–7015, https://doi.org/10.1002/jcp.26623.

[25] Y. Zhu, J. Tan, H. Zhu, et al., Development of kartogenin-conjugated chitosan-hyaluronic acid hydrogel for nucleus pulposus regeneration, Biomater Sci 5 (4) (2017) 784–791, https://doi.org/10.1039/c7bm00001d.

[26] Michael J. Monteiro, Michael F. Cunningham, Polymer nanoparticles via living radical polymerization in aqueous dispersions: design and applications, Macromolecules 45 (12) (2012) 4939–4957, https://doi.org/10.1021/ma300170c.

[27] B. Han, K. Zhu, F.C. Li, et al., A simple disc degeneration model induced by percutaneous needle puncture in the rat tail, Spine 33 (18) (2008) 1925–1934, https://doi.org/10.1097/BRS.0b013e31817c64a9.

[28] C.W. Pfirrmann, A. Metzdorf, M. Zanetti, et al., Magnetic resonance classification of lumbar intervertebral disc degeneration, Spine 26 (17) (2001) 1873–1878, https://doi.org/10.1097/00007632-200109010-00011.

[29] H.J. Mao, Q.X. Chen, B. Han, et al., The effect of injection volume on disc degeneration in a rat tail model, Spine 36 (16) (2011) E1062–E1069, https://doi.org/10.1097/BRS.0b013e3182027d42.

[30] X. Zhou, J. Wang, W. Fang, et al., Genipin cross-linked type II collagen/chondroitin sulfate composite hydrogel-like cell delivery system induces differentiation of adipose-derived stem cells and regenerates degenerated nucleus pulposus, Acta Biomater. 71 (2018) 496–509, https://doi.org/10.1016/j.actbio.2018.03.019.

[31] J. Wang, D. Li, C. Liang, et al., Scar tissue-targeting polymer micelle for spinal cord injury treatment, Small 16 (8) (2020), e1906415, https://doi.org/10.1002/smll.201906415.

[32] C.L. Le Maitre, A.J. Freemont, J.A. Hoyland, Localization of degradative enzymes and their inhibitors in the degenerate human intervertebral disc, J. Pathol. 204 (1) (2004) 47–54, https://doi.org/10.1002/path.1608.

[33] J.J. MacLean, C.R. Lee, M. Alini, et al., The effects of short-term load duration on anabolic and catabolic gene expression in the rat tail intervertebral disc, J. Orthop. Res. 23 (5) (2005) 1120–1127, https://doi.org/10.1016/j.orthres.2005.01.020.

[34] G.W. Omlor, H. Lorenz, K. Engelleiter, et al., Changes in gene expression and protein distribution at different stages of mechanically induced disc degeneration–an in vivo study on the New Zealand white rabbit, J. Orthop. Res. 24 (3) (2006) 385–392, https://doi.org/10.1002/jor.20055.

[35] Y. Han, F. Yuan, C. Deng, et al., Metformin decreases LPS-induced inflammatory response in rabbit annulus fibrosus stem/progenitor cells by blocking HMGB1 release, Aging (Albany NY) 11 (22) (2019) 10252–10265, https://doi.org/10.18632/aging.102453.

[36] M. Tsingas, O.K. Ottone, A. Haseeb, et al., Sox9 deletion causes severe intervertebral disc degeneration characterized by apoptosis, matrix remodeling, and compartment-specific transcriptomic changes, Matrix Biol. 94 (2020) 110–133, https://doi.org/10.1016/j.matbio.2020.09.003.

[37] F. Lv, V.Y. Leung, S. Huang, et al., In search of nucleus pulposus-specific molecular markers, Rheumatology 53 (4) (2014) 600–610, https://doi.org/10.1093/rheumatology/ket303.

[38] J. Zhou, Y. Wang, Y. Liu, et al., Adipose derived mesenchymal stem cells alleviated osteoarthritis and chondrocyte apoptosis through autophagy inducing, J. Cell. Biochem. (2018), https://doi.org/10.1002/jcb.27530.

[39] R. Zuo, Y. Wang, J. Li, et al., Rapamycin induced autophagy inhibits inflammation-mediated endplate degeneration by enhancing Nrf2/Keap1 signaling of cartilage endplate stem cells, Stem Cell. 37 (6) (2019) 828–840, https://doi.org/10.1002/stem.2999.

[40] A. Sotthibundhu, W. Promjuntuek, M. Liu, et al., Roles of autophagy in controlling stem cell identity: a perspective of self-renewal and differentiation, Cell Tissue Res. 374 (2) (2018) 205–216, https://doi.org/10.1007/s00441-018-2829-7.

[41] S. Murakami, H. Motohashi, Roles of Nrf2 in cell proliferation and differentiation, Free Radic. Biol. Med. 88 (Pt B) (2015) 168–178, https://doi.org/10.1016/j.freeradbiomed.2015.06.030.

[42] S.E. Hanson, J. Kim, P. Hematti, Comparative analysis of adipose-derived mesenchymal stem cells isolated from abdominal and breast tissue, Aesthetic Surg. J. 33 (6) (2013) 888–898, https://doi.org/10.1177/1090820X13496115.

[43] X. Zhou, Y. Tao, E. Chen, et al., Genipin-cross-linked type II collagen scaffold promotes the differentiation of adipose-derived stem cells into nucleus pulposus-like cells, J. Biomed. Mater. Res. 106 (5) (2018) 1258–1268, https://doi.org/10.1002/jbm.a.36325.

[44] X. Zhou, C. Ma, B. Hu, et al., FoxA2 regulates the type II collagen-induced nucleus pulposus-like differentiation of adipose-derived stem cells by activation of the Shh signaling pathway, Faseb. J. (2018), fj201800373R, https://doi.org/10.1096/fj.201800373R.

[45] B. Sun, M. Lian, Y. Han, et al., A 3D-Bioprinted dual growth factor-releasing intervertebral disc scaffold induces nucleus pulposus and annulus fibrosus reconstruction, Bioact Mater 6 (1) (2021) 179–190, https://doi.org/10.1016/j.bioactmat.2020.06.022.

[46] Y. Liu, J. Du, P. Peng, et al., Regulation of the inflammatory cycle by a controllable release hydrogel for eliminating postoperative inflammation after discectomy, Bioact Mater 6 (1) (2021) 146–157, https://doi.org/10.1016/j.bioactmat.2020.07.008.

[47] A. Banfi, A. Muraglia, B. Dozin, et al., Proliferation kinetics and differentiation potential of ex vivo expanded human bone marrow stromal cells: Implications for their use in cell therapy, Exp. Hematol. 28 (6) (2000) 707–715, https://doi.org/10.1016/s0301-472x(00)00160-0.

[48] J. Galipeau, M. Krampera, J. Barrett, et al., International Society for Cellular Therapy perspective on immune functional assays for mesenchymal stromal cells as potency release criterion for advanced phase clinical trials, Cytotherapy 18 (2) (2016) 151–159, https://doi.org/10.1016/j.jcyt.2015.11.008.

[49] Y. Huang, T. Jiang, J. Chen, et al., Effects of kartogenin on the attenuated nucleus pulposus cell degeneration of intervertebral discs induced by interleukin-1 beta

and tumor necrosis factor-alpha, Int. J. Mol. Med. 41 (2) (2018) 749–756, https://doi.org/10.3892/ijmm.2017.3283.

[50] Y. Wang, G. Chen, J. Yan, et al., Upregulation of SIRT1 by kartogenin enhances antioxidant functions and promotes osteogenesis in human mesenchymal stem cells, Oxid Med Cell Longev 2018 (2018) 1368142, https://doi.org/10.1155/2018/1368142.

[51] K. Huang, X. Gao, W. Wei, The crosstalk between Sirt1 and Keap1/Nrf2/ARE anti-oxidative pathway forms a positive feedback loop to inhibit FN and TGF-beta 1 expressions in rat glomerular mesangial cells, Exp. Cell Res. 361 (1) (2017) 63–72, https://doi.org/10.1016/j.yexcr.2017.09.042.